Thermophysical Properties of Diphenylmethane and Dicyclohexylmethane as a Reference Liquid Organic Hydrogen Carrier System from Experiments and Molecular Simulations

Manuel Kerscher,[a] *Tobias Klein,*[a] *Peter S. Schulz,*[b] *Emmanouil Veroutis,*[c] *Stefan Dürr,*[b] *Patrick Preuster,*[d] *Thomas M. Koller,*[a] *Michael H. Rausch,**[,a] *Ioannis G. Economou,*[e,f] *Peter Wasserscheid,*[b,d] *Andreas P. Fröba*[a]

[a]Institute of Advanced Optical Technologies − Thermophysical Properties (AOT-TP), Department of Chemical and Biological Engineering (CBI) and Erlangen Graduate School in Advanced Optical Technologies (SAOT), Friedrich-Alexander-University Erlangen-Nürnberg (FAU), Paul-Gordan-Straße 8, 91052 Erlangen, Germany

[b]Institute of Chemical Reaction Engineering (CRT), Department of Chemical and Biological Engineering (CBI), Friedrich-Alexander-University Erlangen-Nürnberg (FAU), Egerlandstraße 3, 91058 Erlangen, Germany

[c]Forschungzentrum Jülich GmbH, IEK-9, Ostring O10, 52425 Jülich, Germany

[d]Forschungszentrum Jülich GmbH, Helmholtz Institute Erlangen-Nürnberg for Renewable Energy (IEK-11), Egerlandstraße 3, 91058 Erlangen, Germany

[e]National Center for Scientific Research "Demokritos", Institute of Nanoscience and Nanotechnology, Molecular Thermodynamics and Modelling of Materials Laboratory, GR-15310 Aghia Paraskevi Attikis, Greece

[f]Texas A&M University at Qatar, Chemical Engineering Program, Education City, PO Box 23874, Doha, Qatar

Emails: manuel.kerscher@fau.de, tobias.klein@fau.de, peter.schulz@fau.de, e.veroutis@fz-juelich.de, stefan.duerr@fau.de, p.preuster@fz-juelich.de, thomas.m.koller@fau.de, michael.rausch@fau.de, ioannis.economou@qatar.tamu.edu, peter.wasserscheid@fau.de, andreas.p.froeba@fau.de

---

*Author to whom correspondence should be addressed. Tel.: +49-9131-85-25898, fax: +49-9131-85-25878, email: michael.rausch@fau.de, ORCID number: 0000-0003-0719-6758.

Supporting Information

Vibrating-Tube Method – Density. The liquid density ρ' was measured at atmospheric pressure of 0.1 MPa with the vibrating-tube instruments DMA 5000 M and DMA 4200 M from Anton Paar. The samples were prepared in the same way as those for the SLS experiments, where syringes were used to fill the samples into the densimeters. Three samples per substance were investigated in each instrument, where each sample was measured as a function of increasing and decreasing temperature. The data from the resulting 6 temperature runs were averaged to obtain the densities reported in Table S1 together with their expanded relative uncertainties.

Table S1. Liquid Density $\rho'(T)$ of DPM and DCM at Temperature T and 0.1 MPa.[a]

T (K)	ρ' (kg·m^{-3})	$100U_r(\rho')$
DPM		
DMA 4200 M		
298.15	1001.32	0.10
303.15	997.49	0.10
323.15	981.88	0.10
348.16	962.15	0.10
373.15	942.52	0.10
398.15	922.77	0.10
423.15	902.71	0.10
448.15	882.87	0.20
473.15	863.04	0.20
DMA 5000 M		
298.15	1001.623	0.01
303.15	997.691	0.01
308.15	993.762	0.01
313.15	989.836	0.01
318.15	985.916	0.01

T (K)	ρ' (kg·m^{-3})	$100U_r(\rho')$
323.15	981.996	0.01
328.15	978.077	0.01
333.15	974.160	0.01
338.15	970.240	0.01
343.15	966.318	0.01
348.15	962.394	0.01
353.15	958.472	0.01
358.15	954.549	0.01
363.15	950.623	0.01
DCM		
DMA 4200 M		
298.15	872.50	0.10
323.15	854.87	0.10
348.15	837.18	0.10
373.15	819.45	0.10
398.15	801.67	0.10
423.15	783.83	0.10
448.15	765.94	0.20
473.15	747.99	0.20
DMA 5000		
283.15	883.056	0.01
288.15	879.540	0.01
293.15	876.022	0.01
298.15	872.501	0.01
303.15	868.979	0.01
308.15	865.454	0.01
313.15	861.928	0.01
318.15	858.399	0.01
323.15	854.869	0.01
328.15	851.336	0.01
333.15	847.802	0.01

T (K)	ρ' (kg·m^{-3})	$100U_r(\rho')$
338.15	844.265	0.01
343.15	840.726	0.01
348.15	837.185	0.01
353.15	833.642	0.01
358.15	830.097	0.01
363.15	826.551	0.01

[a]The expanded uncertainties U are $U(p)$ = 3 kPa as well as $U(T)$ = 0.01 K for the DMA 5000 M and $U(T)$ = 0.03 K for the DMA 4200 M, while the relative expanded uncertainties $U_r(\rho')$ are given in the table (k = 2).

The DMA 5000 M was used starting from 283 K for DCM and from 298 K for DPM up to 363 K in steps of 5 K. It was checked successfully with deionized and degassed water as well as with air before and after each measurement series for a given substance. The maximum relative deviation between individual measurements was 0.005% for DPM and 0.003% for DCM. Considering the complete experimental procedures, the expanded relative uncertainty (k = 2) is estimated to be 0.01% for the results from the DMA 5000 M, where the specified uncertainty of the temperature measurement is 0.01 K.

The DMA 4200 M was used to measure the liquid density from (298 to 473) K in steps of 25 K for DPM and DCM as well as at 303 K for DPM with a specified temperature uncertainty of 0.03 K. Also here, test measurements with air and degassed water were performed successfully before filling a new substance. The instrument was adjusted at 0.1 MPa from (298 to 473) K in steps of 25 K, where air was used as first reference substance for the complete temperature range employing the reference data from Lemmon et al. [1] with an expanded uncertainty (k = 2) of 0.1%. Up to 423 K, the second reference substance was the commercial standard APS600(HT) from Paragon Scientific Ltd. The provided density data certified with an expanded relative uncertainty of 0.01% were checked by measurements with the DMA 5000 M for temperatures from (293 to

363) K, where deviations of less than 0.01% were found. *n*-dodecane with a specified mass fraction purity of $w = 0.99$ purchased from Merck was used as second reference substance for temperatures of (448 and 473) K, where reference data from Lemmon and Huber [2] with an expanded relative uncertainty ($k = 2$) of 0.2% were used. Before the adjustment measurements, more volatile impurities in the *n*-dodecane sample were reduced by applying vacuum at 50 Pa and 323.15 K for about 3 h. Check measurements performed with the DMA 4200 M from (323 to 423) K after adjustment with air and APS600(HT) showed deviations of less than 0.08% from the data of Lemmon and Huber [2]. The maximum relative difference between individual values obtained for the same substance from different experimental runs with the DMA 4200 M was 0.08% for DPM and 0.01% for DCM. The deviations of averaged densities measured with the DMA 4200 M from those obtained with the DMA 5000 M were smaller than 0.03% in most cases. Only for DCM at 298 K, the deviation was 0.09%. Based on the adjustment procedures and the comparison of results as given above, the expanded relative uncertainties of densities measured with the DMA 4200 M are estimated to be 0.1% from (298 to 423) K and 0.2% for (448 and 473) K.

Rotational Viscometry – Dynamic Viscosity. A rotational viscometer (Anton Paar MCR 302) was used together with a coaxial cylindrical double gap measuring system for the determination of the dynamic viscosity at ambient atmosphere of 0.1 MPa at temperatures of 303 K and from (323 to 423) K in steps of 25 K controlled by a counter-cooled Peltier system. An implemented Pt100 class A temperature probe was used to control and measure the temperature with an estimated expanded ($k = 2$) uncertainty of 0.2 K at 303 K up to 0.5 K at 423 K. During the measurements performed for a given sample and temperature, the temperature stability was always better than 0.1 K. Before

each filling with a sample fluid, the double gap measuring system was cleaned with ethanol, acetone and hot deionized water. The samples were used without further treatment.

The measurement procedure included shear rate sweeps where a linear variation of the shear rate was accomplished. The dynamic viscosity was calculated by linear regression of the measured shear stresses as a function of the increasing shear rates during the sweep measurement. The regimes of very small shear rates, where the shear stress is connected with high uncertainties, and high shear rates close to and above the onset of turbulence were excluded for data evaluation. Check measurements performed at constant shear rates as well as sweeps with decreasing shear rates agreed clearly within uncertainties with the results from the procedure described above.

Check measurements were performed with *n*-hexadecane (CAS 544-76-3, Alfa Aesar, mass fraction purity 0.991) and the commercial standard APDEMA-100 (Paragon Scientific, certificate number AP3235) at the same temperatures as for the LOHC samples and covering reference dynamic viscosities from (0.507 to 2.798) mPa·s. In all cases, the deviation from data for a *n*-hexadecane sample from the same supplier measured with SLS [3] (reported maximum expanded relative uncertainty in the temperature range of interest is 2.6%) as well as for the commercial standard from the corresponding certificate (maximum expanded relative uncertainty in the temperature range of interest is 0.32%) was clearly below 5%. The latter value represents also the expanded relative uncertainty of the measurement setup at a confidence level of about 95% according to the manufacturer.

For excluding any degradation effects on the viscosity especially due to oxygenation of the samples in air atmosphere at temperatures up to 423 K, repetition measurements at 323 K were performed after the highest temperature had been investigated. The repetition measurements

agreed with the previously measured data within less than 1% both for the LOHCs and the reference materials.

Force Field Parameters for DPM and DCM. The force field (FF) parameters necessary for the modeling by EMD simulations are summarized in following. For the non-bonded Lennard-Jones (LJ) interactions between two atoms *i* and *j* at a distance r_{ij}, the 12-6 LJ potential of the form $V_{LJ}(r_{ij}) = 4\varepsilon_{LJ}[(\sigma_{LJ}/r_{ij})^{12}-(\sigma_{LJ}/r_{ij})^{6}]$ was used. The energy parameter ε_{LJ} for the L-OPLS-T FF is given here for a temperature of 298.15 K. This value has to be adjusted with respect to temperature according to [4]

$$\varepsilon_{\mathrm{LJ}}(T) = \varepsilon_{\mathrm{LJ,298.15\,K}}\left(1+\sum_{n=0}^{2} C_n T^n\right). \qquad \text{(S1)}$$

In eq S1, $\varepsilon_{\mathrm{LJ,298.15\,K}}$ is the energy parameter given at 298.15 K in the L-OPLS FF [5, 6] and the coefficients are $C_0 = -0.1914$, $C_1 = 8.167\cdot10^{-4}$ K^{-1}, and $C_2 = -5.857\cdot10^{-7}$ K^{-2} [4]. The FF parameters using the L-OPLS-T FF [4-7] are summarized in Table S2 for DPM and in Table S3 for DCM. The FF parameters using the TraPPE FF [8-11] are summarized in Table S4 for DPM and Table S5 for DCM. The labeling of the atoms can be taken from Figure S1. For the TraPPE FF, where hydrogen atoms are not explicitly modeled, the atom types CA, CT, and CR refer to the united-atom interaction sites.

Table S2: FF Parameters for DPM using the L-OPLS-T FF.

atom types	mass (u)	charge (e$^-$)	σ_{LJ} (nm)	ε_{LJ} (kJ·mol^{-1})
CA	12.011	-0.090 / 0.000[a]	0.355	0.29288
HA	1.008	0.090	0.242	0.12552
CT	12.011	-0.148	0.350	0.27614
HC	1.008	0.074	0.250	0.11000

bond stretching	$V_b(r_{ij}) = \frac{1}{2} k_b \left(r_{ij} - r_0\right)^2$		
	bond	k_b (kJ·mol^{-1}·nm^{-2})	r_0 (nm)
	CA-CA	392459.2	0.140
	CA-CT	265265.6	0.151
	CA-HA	307105.6	0.108
	CT-HC	284512.0	0.109
bond angle bending	$V_a(\Theta_{ijk}) = \frac{1}{2} k_a \left(\Theta_{ijk} - \Theta_0\right)^2$		
	bond angle	k_a (kJ·mol^{-1}·rad^{-2})	Θ_0 (°)
	CA-CA-CA	527.184	120.0
	CA-CA-CT	585.760	120.0
	CA-CT-CA	334.720	109.5
	CA-CA-HA	292.880	120.0
	CA-CT-HC	292.880	109.5
	HC-CT-HC	276.144	107.8
dihedral angles	$V_d(\Phi_{ijkl}) = \frac{1}{2}\left[F_1\left(1+\cos\left(\Phi\right)\right) + F_1\left(1-\cos\left(2\Phi\right)\right) + F_3\left(1+\cos\left(3\Phi\right)\right) + F_4\left(1-\cos\left(4\Phi\right)\right)\right]$			
	dihedral angle	F_1 (kJ·mol^{-1})	F_2 (kJ·mol^{-1})	F_3 (kJ·mol^{-1})	F_4 (kJ·mol^{-1})
	CA-CA-CA-CA	30.334	0.000	-30.334	0.000
	CA-CA-CA-CT	30.334	0.000	-30.334	0.000
	CA-CA-CT-CA	30.334	0.000	-30.334	0.000
	CA-CA-CT-HC	0.000	0.000	0.000	0.000
	HA-CA-CA-HA	30.334	0.000	-30.334	0.000
	HA-CA-CA-CA	30.334	0.000	-30.334	0.000

[a]The CA atom, which is bonded to the methyl group, has a partial charge of 0 e$^-$.

Table S3: FF Parameters for DCM using the L-OPLS-T FF.

atom types	mass (u)	charge (e$^-$)	σ_{LJ} (nm)	ε_{LJ} (kJ·mol^{-1})
CR	12.011	-0.148 / -0.074[a]	0.350	0.27614
HR	1.008	0.074	0.250	0.11000
CT	12.011	-0.148	0.350	0.27614
HC	1.008	0.074	0.250	0.11000
bond stretching	$V_b(r_{ij}) = \frac{1}{2} k_b \left(r_{ij} - r_0\right)^2$			
	bond	k_b (kJ·mol^{-1}·nm^{-2})	r_0 (nm)	
	CR-CR	224262.4	0.1529	
	CR-CT	224262.4	0.1529	
	CT-HC	284512.0	0.1090	
	CR-HR	284512.0	0.1090	
bond angle bending	$V_a(\Theta_{ijk}) = \frac{1}{2} k_a \left(\Theta_{ijk} - \Theta_0\right)^2$			
	bond angle	k_a (kJ·mol^{-1}·rad^{-2})	Θ_0 (°)	
	CR-CR-CR	488.27	112.7	
	CR-CR-CT	488.27	112.7	
	CR-CT-CR	488.27	112.7	
	CR-CR-HR	313.80	110.7	

	CR-CT-HC	313.80	110.7
	CT-CR-HR	313.80	110.7
	HC-CT-HC	276.14	107.8
	HR-CR-HR	276.14	107.8

dihedral angles	$V_{\mathrm{d}}(\Phi_{ijkl})=\frac{1}{2}\left[F_1\left(1+\cos\left(\Phi\right)\right)+F_1\left(1-\cos\left(2\Phi\right)\right)+F_3\left(1+\cos\left(3\Phi\right)\right)+F_4\left(1-\cos\left(4\Phi\right)\right)\right]$			
	dihedral angle	F_1 (kJ·mol^{-1})	F_2 (kJ·mol^{-1})	F_3 (kJ·mol^{-1})	F_4 (kJ·mol^{-1})
	CR-CR-CR-CR	2.301	-1.464	0.837	-1.674
	CR-CR-CR-CT	2.301	-1.464	0.837	-1.674
	CR-CR-CT-CR	2.301	-1.464	0.837	-1.674
	CR-CR-CT-HC	0.628	1.883	0.000	-2.510
	HR-CR-CR-HR	0.628	1.883	0.000	-2.510
	HR-CR-CR-CR	0.628	1.883	0.000	-2.510
	CR-CT-CR-HR	0.628	1.883	0.000	-2.510
	CT-CR-CR-HR	0.628	1.883	0.000	-2.510
	HR-CR-CT-HC	0.628	1.883	0.000	-2.510

[a]The CR atom, which is bonded to the methyl group connecting the two cyclohexyl rings, has a partial charge of -0.074 e$^-$.

Table S4: FF Parameters for DPM using the TraPPE FF.

atom types	mass (u)	charge (e$^-$)	σ_{LJ} (nm)	$\varepsilon_{\mathrm{LJ}}$ (kJ·mol^{-1})
CA	13.019 / 12.011[a]	0.000	0.468	0.08314
CT	14.027	0.000	0.395	0.38247

bond stretching	$V_{\mathrm{b}}(r_{ij})=\frac{1}{2}k_{\mathrm{b}}\left(r_{ij}-r_0\right)^2$		
	bond	k_b (kJ·mol^{-1}·nm^{-2})	r_0 (nm)
	CA-CA	392459.2	0.154
	CA-CT	265265.6	0.154

bond angle bending	$V_{\mathrm{a}}(\Theta_{ijk})=\frac{1}{2}k_a\left(\Theta_{ijk}-\Theta_0\right)^2$		
	bond angle	k_a (kJ·mol^{-1}·rad^{-2})	Θ_0 (°)
	CA-CA-CA	527.184	120.0
	CA-CA-CT	585.760	120.0
	CA-CT-CA	334.720	109.5

dihedral angles	$V_{\mathrm{d}}(\Phi_{ijkl})=\frac{1}{2}\left[F_1\left(1+\cos\left(\Phi\right)\right)+F_1\left(1-\cos\left(2\Phi\right)\right)+F_3\left(1+\cos\left(3\Phi\right)\right)+F_4\left(1-\cos\left(4\Phi\right)\right)\right]$			
	dihedral angle	F_1 (kJ·mol^{-1})	F_2 (kJ·mol^{-1})	F_3 (kJ·mol^{-1})	F_4 (kJ·mol^{-1})
	CA-CA-CA-CA	30.334	0.000	-30.334	0.000
	CA-CA-CA-CT	30.334	0.000	-30.334	0.000
	CA-CA-CT-CA	30.334	0.000	-30.334	0.000

[a]The CA atom, which is bonded to the methyl group, has a mass of 12.011 u.

Table S5: FF Parameters for DCM using the TraPPE FF.

atom types	mass (u)	charge (e^-)	σ_{LJ} (nm)	ε_{LJ} (kJ·mol^{-1})
CR	14.027 / 13.019[a]	0.000	0.391	0.43651
CT	14.027	0.000	0.395	0.38247
bond stretching	$V_b(r_{ij}) = \frac{1}{2} k_b \left(r_{ij} - r_0\right)^2$			
	bond	k_b (kJ·mol^{-1}·nm^{-2})		r_0 (nm)
	CR-CR	392459.2		0.154
	CR-CT	265265.6		0.154
bond angle bending	$V_a(\Theta_{ijk}) = \frac{1}{2} k_a \left(\Theta_{ijk} - \Theta_0\right)^2$			
	bond angle	k_a (kJ·mol^{-1}·rad^{-2})		Θ_0 (°)
	CR-CR-CR	519.653		114.0
	CR-CR-CT	519.653		114.0
	CR-CT-CR	519.653		114.0
dihedral angles	$V_d(\Phi_{ijkl}) = \frac{1}{2}\left[F_1\left(1+\cos\left(\Phi\right)\right) + F_1\left(1-\cos\left(2\Phi\right)\right) + F_3\left(1+\cos\left(3\Phi\right)\right) + F_4\left(1-\cos\left(4\Phi\right)\right)\right]$			
	dihedral angle	F_1 (kJ·mol^{-1})	F_2 (kJ·mol^{-1})	F_3 (kJ·mol^{-1})	F_4 (kJ·mol^{-1})
	CR-CR-CR-CR	42.179	-56.871	29.175	-0.5238
	CR-CR-CR-CT	42.179	-56.871	29.175	-0.5238
	CR-CR-CT-CR	42.179	-56.871	29.175	-0.5238

[a]The CR atom, which is bonded to the methyl group connecting the two cyclohexyl rings, has a mass of 13.019 u.

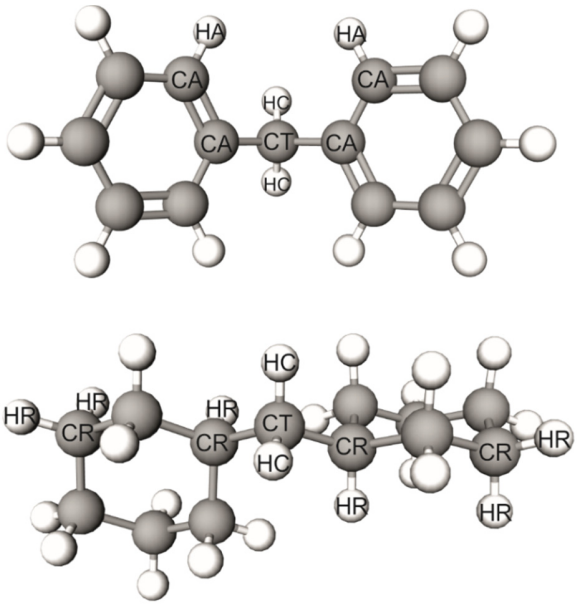

Figure S1: Atom types in DPM (upper part) and DCM (lower part). In DPM, carbon and hydrogen atoms within the phenyl rings are atom type CA and HA. In DCM, the carbon and hydrogen atoms within the cyclohexyl rings are atom type CR and HR. In both cases, the methyl group connecting the rings are built from the atom types CT and HC.

Conformational Analysis. An experimental conformational analysis was performed for DPM and DCM using the NMR-1 equipment detailed in the main text. In the following, the measurement procedure for the conformational analysis is outlined.

Conformational analysis was performed on the basis of the dihedral angles as obtained from the Karplus equation [12] with the constants A = 7.76 Hz, B = -1.1 Hz, and C = 1.4 Hz, for three-bond vicinal ^{3}J couplings. For benzene, it has been shown that the ortho-carbon exhibits a three-bond coupling to the para-protons in the range of $^{3}J_{CH}$ = (7-8) Hz [13-15]. Two- and four-bond couplings to the meta-protons are much smaller and on the order of $^{2,4}J_{CH}$ = 1 Hz.

Therefore, by analyzing the ^{13}C-^{1}H coupled spectrum of DPM (Figure S2), the observed couplings of (6.5, 5.2 and 5.1) Hz are attributed to the three-bond connectivity of the ortho-carbon to the methylene protons. Due to second-order effects, the resulting multiplets are slightly asymmetric and give rise to slightly different couplings, as can be observed from the expanded spectrum in Figure S2. Nevertheless, taking the average over these couplings yields a value of 5.6 Hz, which corresponds to average dihedral angles of (~36 and ~132)°.

For DCM, the three-bond coupling of the methylene protons to the proton in the –CH group was used. Analysis of the ^{1}H spectrum as shown in Figure S3 reveals a value of $^{3}J_{HH}$ = 7 Hz, which corresponds to average angles of (~22.6 and ~141)°.

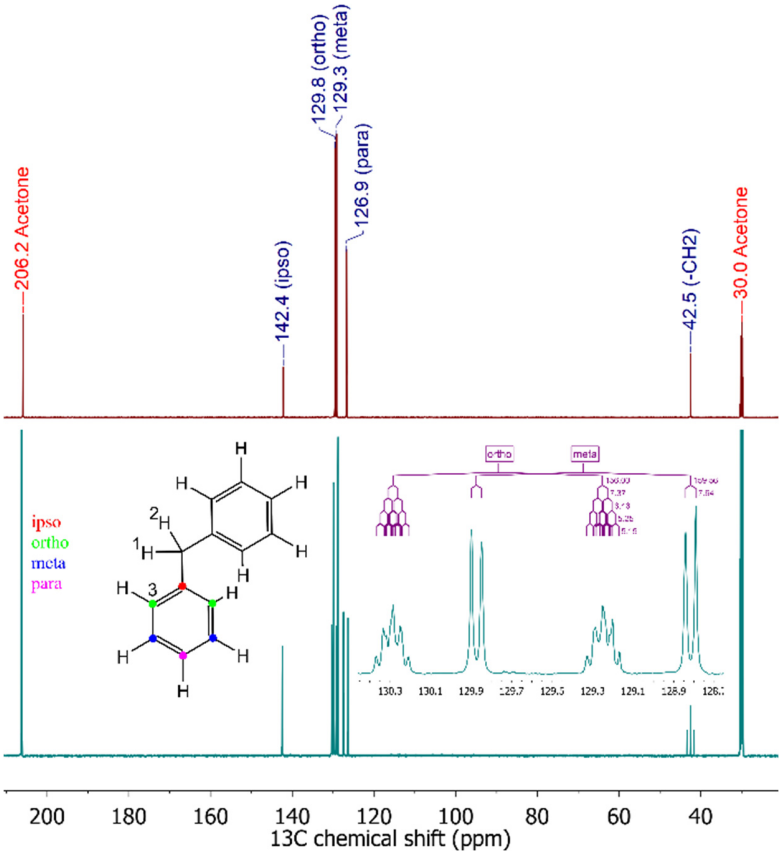

Figure S2. ^{13}C NMR (151 MHz, ~100 mg DPM in 0.75 ml Acetone-d$_6$, 293 K) δ 142.42 (p, $^3J_{CH}$ = 7.0 Hz), 129.77 (dp, $^1J_{CH}$ = 156.0, $^3J_{CH}$ = 7.4, 6.5, 5.2, 5.1 Hz), 129.35 (dd, $^1J_{CH}$ = 159.6, $^3J_{CH}$ = 7.6 Hz), 126.91 (dt, $^1J_{CH}$ = 160.7, $^3J_{CH}$ = 7.3 Hz), 42.52 (tp, $^1J_{CH}$ = 127.2, $^3J_{CH}$ = 4 Hz). Multiplets are assigned according to the resolved peaks in the spectrum. The upper spectrum is the ^{1}H decoupled one, the lower spectrum is the ^{1}H coupled one. The inset indicates the spectrum for the region corresponding to the orto- and meta-carbons as well as their ^1J and ^3J couplings.

Due to the presence of two hydrogen atoms in the methylene group of DPM and DCM, the resulting coupling value represents an average value of multiple contributions. The observed ^3J corresponds therefore to a population-weighted average of the individual couplings, i.e. $^3J_{obs} = (\alpha \cdot {}^3J_{1,2} + \beta \cdot {}^3J_{2,3})/2$, where α, β are the populations of each conformation and indices 1 to 3 correspond to the participating protons or carbons, as shown in Figures S2 and S3.

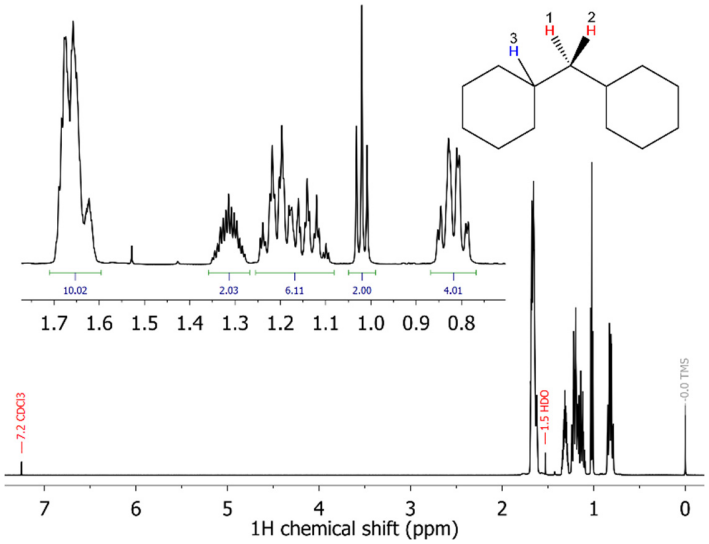

Figure S3. ^{1}H NMR (600 MHz, ~90 mg DCM in 0.75 ml $CDCl_3$, 293 K) δ 1.71 – 1.60 (m, 10H), 1.31 (ttt, J = 10.6, 6.8, 3.3 Hz, 2H), 1.25 – 1.08 (m, 6H), 1.02 (t, J = 7.0 Hz, 2H), 0.82 (qd, J = 12.9, 11.8, 3.8 Hz, 4H). The molecular structure indicates the protons of the methylene group (red) which are coupled to the –CH proton (blue).

In order to investigate whether the fluid structure of DPM and DCM can be captured by the L-OPLS-T FF, the same dihedral angles as studied in the NMR experiments were calculated from EMD simulations in the liquid phase.

For DPM, the dihedral angles between the hydrogen of the methylene group and the carbon atoms at the ortho position of the phenyl rings at a temperature of 303.15 K were calculated in accordance to the NMR experiments. In total, eight different dihedral angles can be calculated for each molecule at every given time step. In order to compare the dihedral angles to the results from NMR measurements, which were calculated from coupling constants using the Karplus equation [12], the eight different dihedral angles were averaged. The probability distribution of the dihedral angle as well as the angle calculated from NMR experiments are shown in the upper part of Figure S4. The probability function shows two pairs of distinct peaks at (+37 and −37)° and (+77 and −77)°. In EMD simulation, positive and negative dihedral angles are possible, where the sign

depends only on the order of the four atoms, which define a dihedral angle. This means that the dihedral angle between atoms 1-2-3-4 has the same absolute value but the opposite sign of the dihedral angle defined by the same atoms with the order 4-3-2-1. Since in the NMR experiments only the absolute value of the dihedral angle can be accessed, in the following discussion only the absolute values of the dihedral angles from EMD simulations are mentioned. For DPM, this means that only two different dihedral angles of (37 and 77)° can be found. The value of 37° is in very good agreement with the absolute value of 36° measured with NMR experiments. The presence of a second peak at 77° is due to the fact that the planes of the phenyl ring are not parallel. This angle between the phenyl rings was calculated to be about 40° for DPM and is shown in Figure S5.

For DCM, two very distinct dihedral angles were found with values of about (60 and 180)°. In order to compare these values to the NMR experiments, the Karplus equation [12] was used to calculate the coupling values. For angles of (60 and 180)°, this would correspond to coupling of (2.79 and 10.26) Hz, respectively. Due to the fact that the coupling measured by NMR is the average of these two values, the simulated angles correspond to an average coupling of 6.5 Hz, which is in good agreement with the value of 7 Hz measured by NMR.

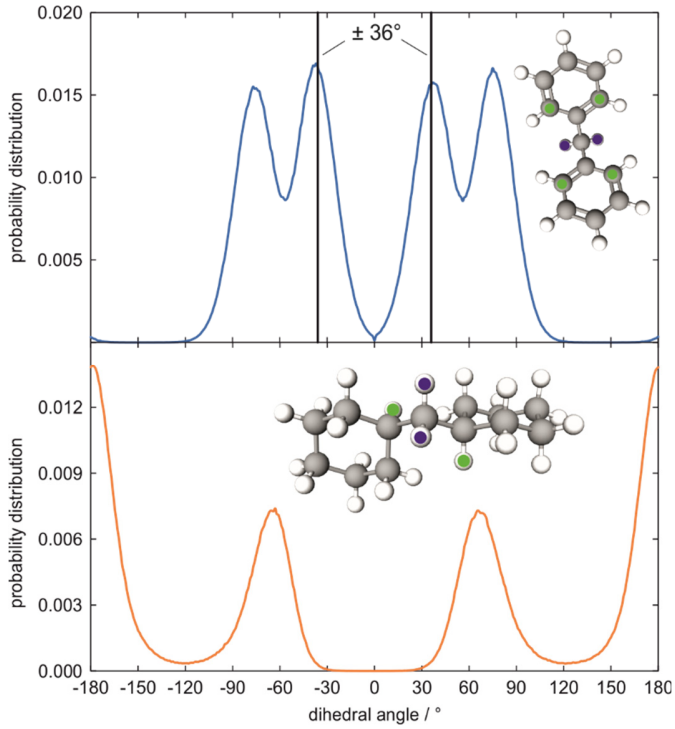

Figure S4. Probability distribution of the dihedral angle connecting the methylene hydrogen with the carbon atom at the ortho position in the phenyl ring in the case of DPM (upper part). For DCM (lower part), the probability function for the dihedral angle between the methylene hydrogen and the hydrogen bond to the carbon at the ipso position of the cyclohexyl ring is shown. In both cases, the dihedral angles were evaluated from EMD simulations in the liquid phase at 303.15 K.

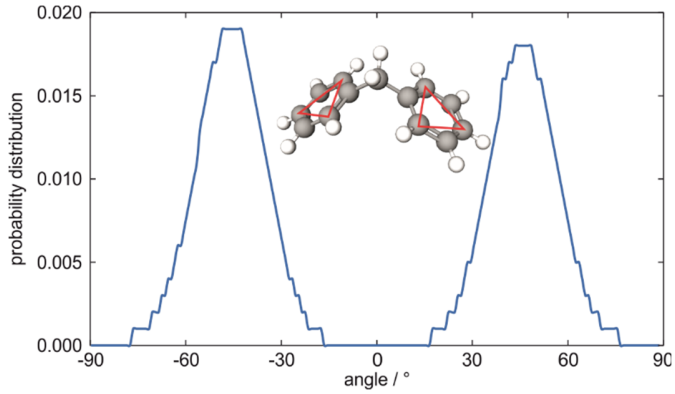

Figure S5. Probability distribution of the angle between the two planes of the phenyl rings in DPM at 298.15 K from EMD simulations.

Summary of EMD Results. Table S6 summarizes the EMD simulation results and expanded statistical uncertainties (k = 2) for the densities ρ', dynamic viscosities η' and self-diffusion coefficients D'_{self} in the compressed liquid phase close to saturation conditions as well as surface tensions σ at vapor-liquid equilibrium (VLE) conditions of DPM and DCM using the L-OPLS-T FF at temperatures between (303.15 and 623.15) K.

Table S6. Densities ρ', Dynamic Viscosities η', and Self-Diffusion Coefficients D'_{self} in the Compressed Liquid Phase Close to Saturation Conditions as Well as Surface Tensions σ at VLE Conditions of DPM and DCM from EMD Simulations. Expanded Statistical Relative or Absolute Uncertainties (k = 2) are Included for All Simulated Properties.

T (K)	ρ' (kg·m^{-3})	100 $U_r(\rho')$	η' (mPa·s)	100 $U_r(\eta')$	σ (mN·m^{-1})	100 $U_r(\sigma)$	10^9 D′ (m^2·s^{-1})	100 $U_r(D')$
DPM								
303.15	975.6	0.08	3.22	14	38.0	13	0.313	2.7
323.15	958.9	0.03	2.17	6.0	36.4	4.6	0.541	2.1
373.15	924.6	0.03	1.08	6.4	32.0	9.2	1.28	3.2
423.15	891.3	0.03	0.612	4.1	28.4	2.2	2.35	2.2
473.15	854.6	0.06	0.371	17	24.2	1.4	3.89	2.6
523.15	818.2	0.04	0.244	17	20.5	1.5	6.01	1.2
573.15	777.3	0.08	0.197	4.9	16.4	6.5	8.48	2.5
623.15	730.5	0.13	0.125	13	12.1	3.6	12.6	3.2
DCM								
303.15	861.0	0.04	6.47	7.5	31.7	7.0	0.173	6.5
323.15	846.4	0.05	4.01	5.1	29.3	9.1	0.308	6.4
373.15	810.5	0.10	1.52	8.7	26.5	3.1	0.853	5.4
423.15	774.8	0.04	0.770	13	22.0	6.4	1.76	6.8
473.15	737.7	0.04	0.416	10	17.8	4.7	3.13	7.7
523.15	698.9	0.12	0.244	22	15.1	5.5	5.08	2.9
573.15	656.8	0.07	0.176	21	10.8	9.0	7.96	7.6
623.15	606.6	0.16	0.0978	17	6.58	7.0	13.1	8.5

REFERENCES

[1] Lemmon EW, Jacobsen RT, Penoncello SG, Friend DG. Thermodynamic properties of air and mixtures of nitrogen, argon, and oxygen from 60 to 2000 K at pressures to 2000 MPa. J Phys Chem Ref Data. 2000;29:331-385. https://doi.org/10.1063/1.1285884.

[2] Lemmon EW, Huber ML. Thermodynamic properties of *n*-dodecane. Energy & Fuels. 2004;18:960-967. https://doi.org/10.1021/ef0341062.

[3] Klein T, Yan S, Cui J, Magee JW, Kroenlein K, Rausch MH, Koller TM, Fröba AP. Liquid viscosity and surface tension of *n*-hexane, *n*-octane, *n*-decane, and *n*-hexadecane up to 573 K by surface light scattering. J Chem Eng Data. 2019;64:4116-4131. https://doi.org/10.1021/acs.jced.9b00525.

[4] Klein T, Lenahan FD, Kerscher M, Rausch MH, Economou IG, Koller TM, Fröba AP. Characterization of long linear and branched alkanes and alcohols for temperatures up to 573.15 K by surface light scattering and molecular dynamics simulations. J Phys Chem B. 2020;124:4146-4163. https://doi.org/10.1021/acs.jpcb.0c01740.

[5] Siu SWI, Pluhackova K, Böckmann RA. Optimization of the OPLS-AA force field for long hydrocarbons. J Chem Theory Comput. 2012;8:1459-1470. https://doi.org/10.1021/ct200908r.

[6] Pluhackova K, Morhenn H, Lautner L, Lohstroh W, Nemkovski KS, Unruh T, Böckmann RA. Extension of the LOPLS-AA force field for alcohols, esters, and monoolein bilayers and its validation by neutron scattering experiments. J Phys Chem B. 2015;119:15287-15299. https://doi.org/10.1021/acs.jpcb.5b08569.

[7] Jorgensen WL, Maxwell DS, Tirado-Rives J. Development and testing of the OPLS all-atom force field on conformational energetics and properties of organic liquids. J Am Chem Soc. 1996;118:11225-11236. https://doi.org/10.1021/ja9621760.

[8] Martin MG, Siepmann JI. Transferable potentials for phase equilibria. 1. United-atom description of *n*-alkanes. J Phys Chem B. 1998;102:2569-2577. https://doi.org/10.1021/jp972543+.

[9] Martin MG, Siepmann JI. Novel configurational-bias monte carlo method for branched molecules. Transferable potentials for phase equilibria. 2. United-atom description of branched alkanes. J Phys Chem B. 1999;103:4508-4517. https://doi.org/10.1021/jp984742e.

[10] Rai N, Siepmann JI. Transferable potentials for phase equilibria. 9. Explicit hydrogen description of benzene and five-membered and six-membered heterocyclic aromatic compounds. J Phys Chem B. 2007;111:10790-10799. https://doi.org/10.1021/jp073586l.

[11] Keasler SJ, Charan SM, Wick CD, Economou IG, Siepmann JI. Transferable potentials for phase equilibria–united atom description of five- and six-membered cyclic alkanes and ethers. J Phys Chem B. 2012;116:11234-11246. https://doi.org/10.1021/jp302975c.

[12] Karplus M. Vicinal proton coupling in nuclear magnetic resonance. J Am Chem Soc. 1963;85:2870-2871. https://doi.org/10.1021/ja00901a059.

[13] Weigert FJ, Roberts JD. Nuclear magnetic resonance spectroscopy. Benzene-^{13}C. J Am Chem Soc. 1967;89:2967-2969. https://doi.org/10.1021/ja00988a029.

[14] Weigert FJ, Roberts JD. Nuclear magnetic resonance spectroscopy, long-range spin-spin couplings involving carbon-13. J Am Chem Soc. 1969;91:4940-4941. https://doi.org/10.1021/ja01045a070.

[15] Äyräs P, Laatikainen R, Lötjönen S. The ^{13}C,H coupling constants in structural and conformational analysis. IV–the rotational dependence of the long-range CH couplings of the aldehyde and hydroxyl protons in salicylaldehyde. Organ Magnet Res. 1980;13:387-390. https://doi.org/10.1002/mrc.1270130520.